Supplementary Information

Reconfigurable ultrafast perovskite polariton logic gates via nonlinear dynamics

Yuyang Zhang[1,#], Zhuoya Zhu[2,3,#], Xin Zeng[2], Shuai Zhang[2], Xinyi Deng[1], Tian Lan[1], Changhai Zhu[1], Kwok Kwan Tang[1], Qinglin Jia[1], Yuexing Xia[2,3], Yiyang Gong[2,3], Wenna Du[2,3], Feng Li[4], Rui Su[5], Xuekai Ma[6], Xinfeng Liu[2,3,*] and Qing Zhang[1,*]

[1]School of Materials Science and Engineering, Peking University, Beijing 100871, China

[2]CAS Key Laboratory of Standardization and Measurement for Nanotechnology, CAS Center for Excellence in Nanoscience, National Center for Nanoscience and Technology, Beijing 100190, China

[3]University of Chinese Academy of Sciences, Beijing 100049, China

[4]Key Laboratory for Physical Electronics and Devices of the Ministry of Education & Shaanxi Key Lab of Information Photonic Technique, School of Electronic Science and Engineering, Faculty of Electronic and Information Engineering, Xi'an Jiaotong University, Xi'an 710049, China

[5]Division of Physics and Applied Physics, School of Physical and Mathematical Sciences, Nanyang Technological University, Singapore 637371, Singapore

[6]Department of Physics and Center for Optoelectronics and Photonics Paderborn (CeOPP), Paderborn University, Warburger Strasse 100, Paderborn 33098, Germany

[*]Email address: q_zhang@pku.edu.cn; liuxf@nanoctr.cn;

[#]These authors contributed equally to this work.

Contents

1. Materials and microcavity fabrication

$CsPbBr_3$ microwires were prepared by a chemical vapor deposition (CVD) process. Briefly, 10 mg of CsBr and 20 mg of $PbBr_2$ powders (99.999%, Sigma-Aldrich) were mixed, loaded into a quartz boat, and placed in a tube furnace (Lindberg/Blue M TF55035C-1). Three Si wafers ((100) plane, 1 × 1 cm^2) were positioned 25 cm downstream from the precursor boat. After the chamber was evacuated for 2 h, high-purity N_2 (99.99%) was introduced at a flow rate of 30 sccm to stabilize the pressure at 400 Torr. The furnace temperature was then raised to 575 °C over 20 min and maintained for 10 min, yielding $CsPbBr_3$ microwires on the Si substrates.

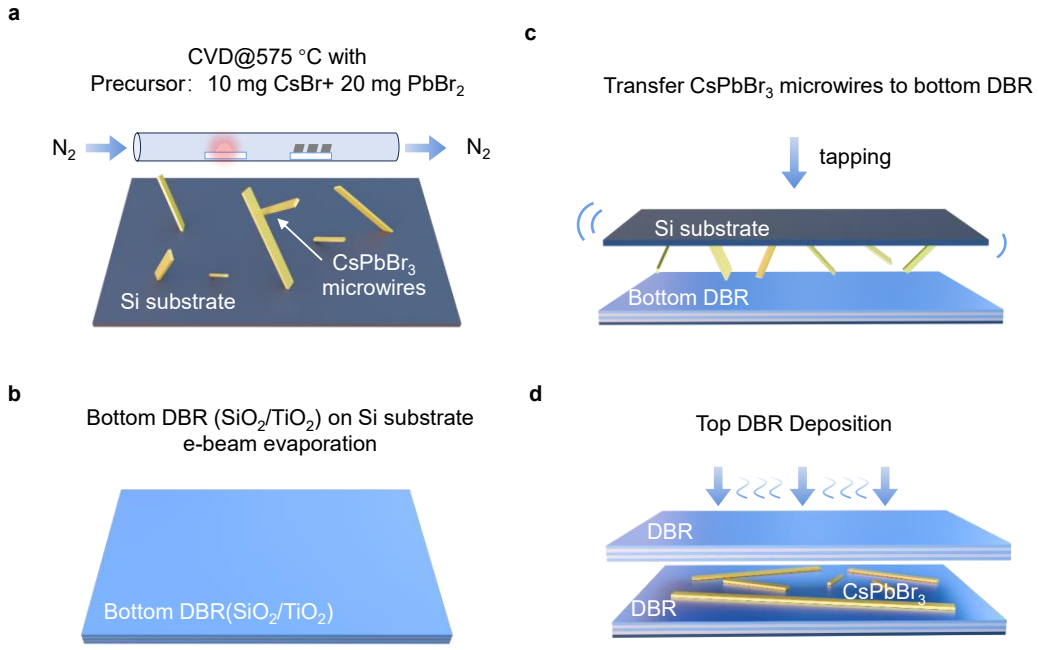

Figure S1 Fabrication and cavity integration of $CsPbBr_3$ microwires. (a) Schematic illustration of CVD growth of $CsPbBr_3$ microwires on Si substrates. **(b)** Bottom DBR on Si substrate, consisting of 19.5 pairs of TiO_2/SiO_2 layers deposited by e-beam evaporation. **(c)** Mechanical transfer of the $CsPbBr_3$ microwires onto the bottom dielectric DBR by gentle contact and light tapping. **(d)** Fabry-Pérot microcavity encapsulation by deposition of the SiO_2 spacer layer and the top DBR.

The microcavity was constructed by embedding the perovskite into two dielectric distributed Bragg reflector (DBR) fabricated by electron-beam evaporation. For the bottom DBR, 19.5 pairs of TiO_2 (54 nm)/SiO_2 (88 nm) layers were deposited on Si wafers, followed by an additional SiO_2 layer for cavity-length adjustment. The $CsPbBr_3$ microwires were then mechanically transferred from the Si substrate onto the bottom DBR by gentle tapping, thereby releasing the microwires

onto the DBR surface. After transfer, a SiO_2 spacer layer was deposited as a protective and cavity-spacing layer. The cavity was finally completed by depositing the top DBR, consisting of 9.5 pairs of SiO_2/TiO_2 layers with the same thicknesses as those of the bottom DBR.

2. Morphology characterization of $CsPbBr_3$

The morphology of the $CsPbBr_3$ microwires was characterized by scanning electron microscopy (SEM, Hitachi SU8220) and atomic force microscopy (AFM, Veeco Dimension 3100, tapping mode). SEM images of the $CsPbBr_3$ microwires grown on Si substrates reveal clean and uniform surfaces. The microwires exhibit widths ranging from hundreds of nanometres to several micrometres and lengths from several to ~30 micrometres. AFM analysis further confirms a thickness of 233 nm and a root-mean-square roughness of ~0.97 nm. These structural characteristics provide a suitable basis for optical confinement and one-dimensional polariton propagation.

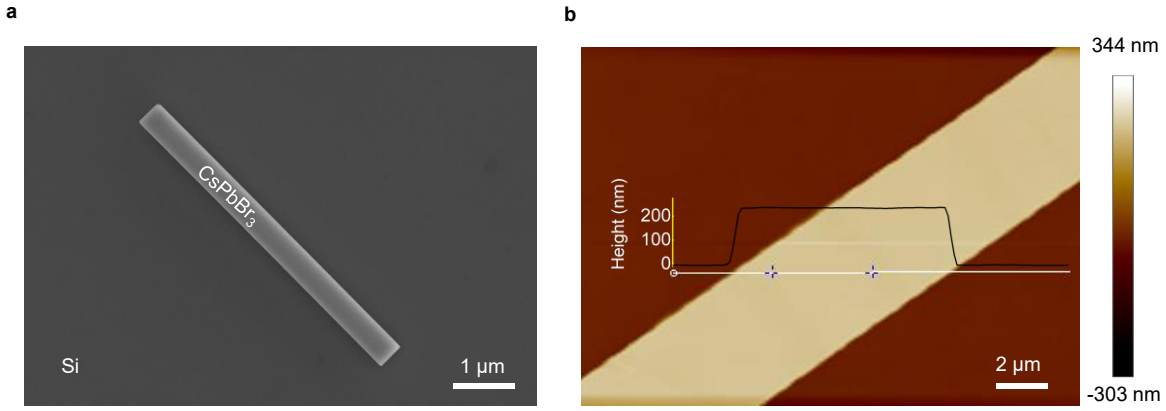

Figure S2 Morphological characterizations of $CsPbBr_3$ microwires. (a) SEM image of a representative $CsPbBr_3$ microwire. Scale bar: 1 μm. **(b)** AFM image and corresponding height profile along the marked line, showing a thickness of 233 nm and a root-mean-square roughness of ~0.97 nm. Scale bar: 2 μm.

3. Photoluminescence properties of $CsPbBr_3$

Steady-state photoluminescence was collected under 405 nm continuous-wave (CW) excitation with a power of 1.7 μW through a ×100 objective (Olympus, NA = 0.9), and the emission was collected by a liquid-nitrogen-cooled spectrometer (SP2500i, Princeton Instruments). Time-resolved photoluminescence was collected using a 515 nm pulsed laser obtained by frequency doubling a 1030 nm laser operating at 10 kHz, and the decay curve was collected with a time-correlated single-photon-counting spectrometer. The decay curve was fitted with a triple-exponential function：

$$I(t) = y_0 + A_1 e^{-t/t_1} + A_2 e^{-t/t_2} + A_3 e^{-t/t_3}$$

Here, y_0 represents the background offset. The decay curve is fitted with a triple-exponential function to account for multiple recombination channels, including fast surface or trap-assisted non-radiative recombination, intermediate excitonic recombination, and slower recombination processes associated with deep trap states. The average lifetime is calculated as $\tau = A_1 t_1 + A_2 t_2 + A_3 t_3$ yielding a value of 7.57 ± 0.11 ns.

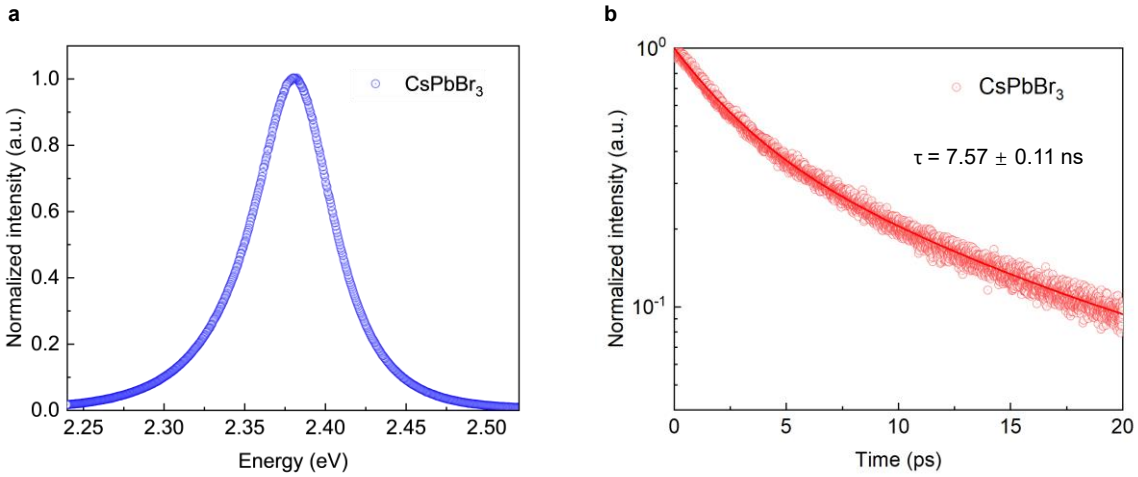

Figure S3 Steady-state and time-resolved photoluminescence of $CsPbBr_3$. (a) Steady-state photoluminescence spectrum of a $CsPbBr_3$ under 405 nm CW excitation at room temperature, showing a peak centered at 2.38 eV with a Gaussian profile. **(b)** Time-resolved photoluminescence decay of a $CsPbBr_3$ microwire under 515 nm, 10 kHz pulsed excitation at room temperature. The decay is fitted with a triple-exponential function, yielding an average lifetime of 7.57 ± 0.11 ns.

4. Strong coupling of exciton and photon

To identify the strong coupling between excitons and photons in the $CsPbBr_3$ microcavity, angle-resolved photoluminescence spectra were collected under 405 nm CW excitation at room temperature. The spectra were collected using a home-built Fourier-space imaging system. The energy–momentum dispersion was fitted using a coupled-oscillator model describing the interaction between the cavity photon mode and the exciton state:

$$E_{\mathrm{UPB,LPB}}(k) = \frac{E_{ph} + E_{\mathrm{x}}}{2} \pm \frac{1}{2}\sqrt{4g^2 + [(E_c - E_x))]^2}$$

where E_{UPB} and E_{LPB} are the energies of the upper and lower polariton branches, E_{ph} and E_{X} are the energies of the cavity-photon mode and exciton state, respectively, and g is the exciton–photon coupling strength. The fitting yields an exciton energy E_{X} = 2.39 eV, a cavity-photon energy E_{ph} = 2.285 eV at k = 0, and a Rabi splitting energy of 130 meV. The corresponding photonic and excitonic fractions of the LPB were further extracted from the coupled-oscillator model:

$$|X_{\mathrm{L}}|^2 = \frac{1}{2}\left(1 + \frac{\delta_{\mathrm{k}}}{\sqrt{\hbar^2\Omega^2 + \delta_{\mathrm{k}}^2}}\right), |C_{\mathrm{L}}|^2 = \frac{1}{2}\left(1 - \frac{\delta_{\mathrm{k}}}{\sqrt{\hbar^2\Omega^2 + \delta_{\mathrm{k}}^2}}\right)$$

where $\delta_{\mathrm{k}} = E_{\mathrm{ph}} - E_{\mathrm{X}}$, X_{L} and C_{L} denote the excitonic and photonic fractions of the LPB, respectively, and Ω is the Rabi splitting extracted from the dispersion fitting above. A large photonic fraction leads to significant energy broadening of the LPB, resulting in more clearly separated energy levels that facilitate reliable logic gate discrimination.

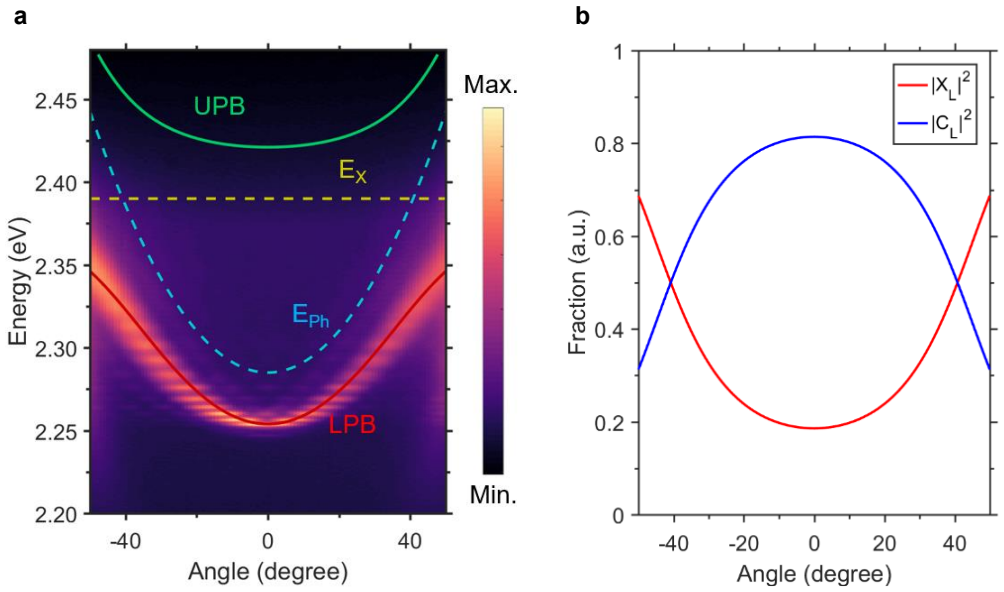

Figure S4 Strong coupling of exciton and photon in the microcavity. (a) Angle-resolved photoluminescence spectrum of the $CsPbBr_3$ microcavity under 405 nm CW excitation at room temperature, together with the fitted LPB, UPB, cavity-photon mode, and exciton energy. The LPB exhibits multiple discrete polariton channels under one-dimensional confinement. **(b)** Photonic (blue line) and excitonic (red line) fractions of the LPB extracted from the coupled-oscillator model.

5. Real-space and k-space EP condensates

We next investigate EP condensation in the ring-shaped optical trap. The ring-shaped excitation creates exciton-induced potential barriers on both sides, which, due to the repulsive interaction between excitons and polaritons, drive counter-propagating polariton flows toward the trap center. Upon reaching the threshold, real-space condensation emerges within the interior of the excitation ring. Power-dependent real-space optical images and angle-resolved photoluminescence spectra were collected under 400 nm pulsed excitation at a repetition rate of 1 kHz at room temperature to track the evolution of the polariton emission with increasing pump power. As the excitation power increases, localized condensates appear in real space, while in momentum-energy space, the emission exhibits discrete energy levels with narrow linewidths, accompanied by a pronounced energy blueshift.

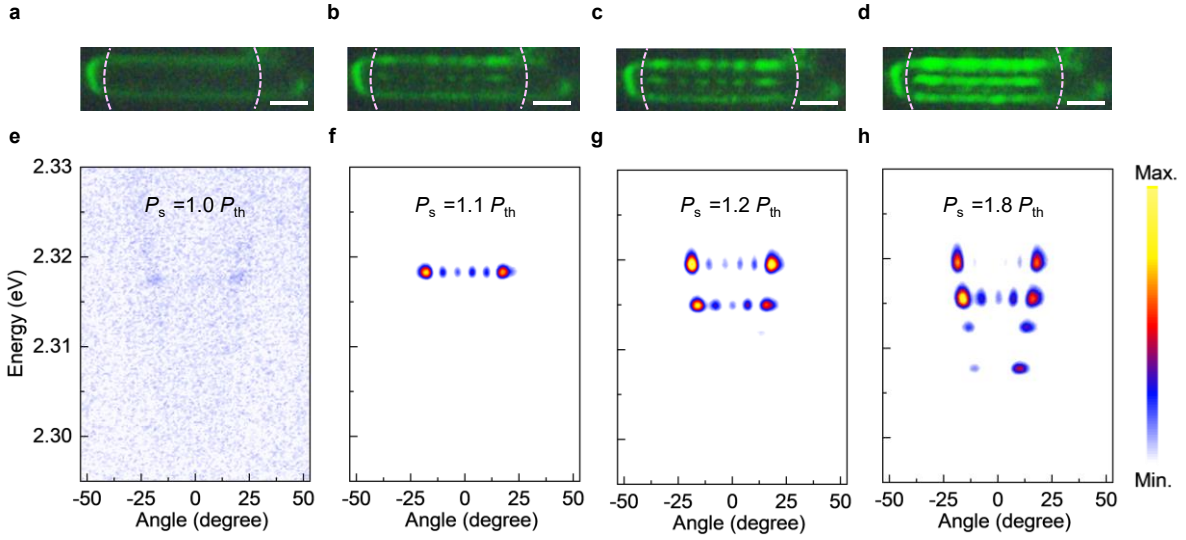

Figure S5 Power-dependent real-space optical images and angle-resolved photoluminescence spectra of EP condensates. (a–d) Real-space optical images collected under four representative excitation powers. Scale bar: 2 μm. The light purple dashed line indicates the position of the signal beam. **(e–h)** Corresponding angle-resolved photoluminescence spectra under the same excitation conditions. Excitation source: 400 nm pulsed laser, 1 kHz, at room temperature.

6. Evolution of intensity, linewidth and blueshift of EP condensates

To further quantify the condensation process, we extracted the integrated emission intensity, full width at half maximum (FWHM), and emission energy as functions of excitation power. When the pump power reaches the threshold, the photoluminescence intensity increases sharply by nearly one order of magnitude, driven by the stimulated scattering of polaritons. Meanwhile, the linewidth exhibits a rapid narrowing. As the excitation power is further increased, enhanced polariton–polariton and exciton–polariton interactions give rise to a monotonic blueshift of the emission energy. These features further confirm the formation of EP condensates.

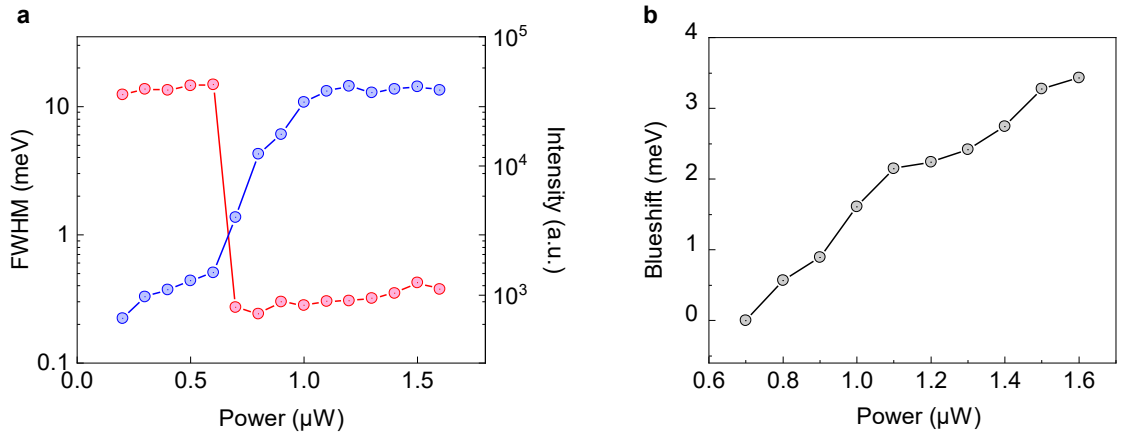

Figure S6 Power-dependent evolution across the condensation threshold. (a) Emission intensity and FWHM as functions of excitation power under 400 nm pulsed excitation at room temperature. **(b)** Energy blueshift as a function of excitation power.

7. The spatial and temporal coherence of the EP condensates

The establishment of coherence provides an additional signature of exciton–polariton condensation. The first-order coherence of the EP condensates was examined using a home-built Michelson interferometer under 1 kHz pulsed excitation at room temperature. The emitted signal was split by a 50:50 beam splitter into two paths, referred to as the left arm and right arm. After being reflected by the corresponding reflectors, the two beams were recombined and projected onto a CMOS camera to generate interference images. Above the threshold, the formation of the polariton condensate gives rise to well-defined spatial interference fringes. The fringe visibility is extracted as：

$$V(t) = \frac{I_{max} - I_{min}}{I_{max} + I_{min}}$$

reaching a value of ~0.6. By tuning the position of one reflector using a piezoelectric stage, the temporal evolution of the visibility was further collected, yielding a coherence time of 7.58 ps. Together with the power-dependent characteristics discussed above, the observed spatial and temporal coherence confirms the formation of EP condensates and their coherent lasing behavior within the ring-shaped optical trap.

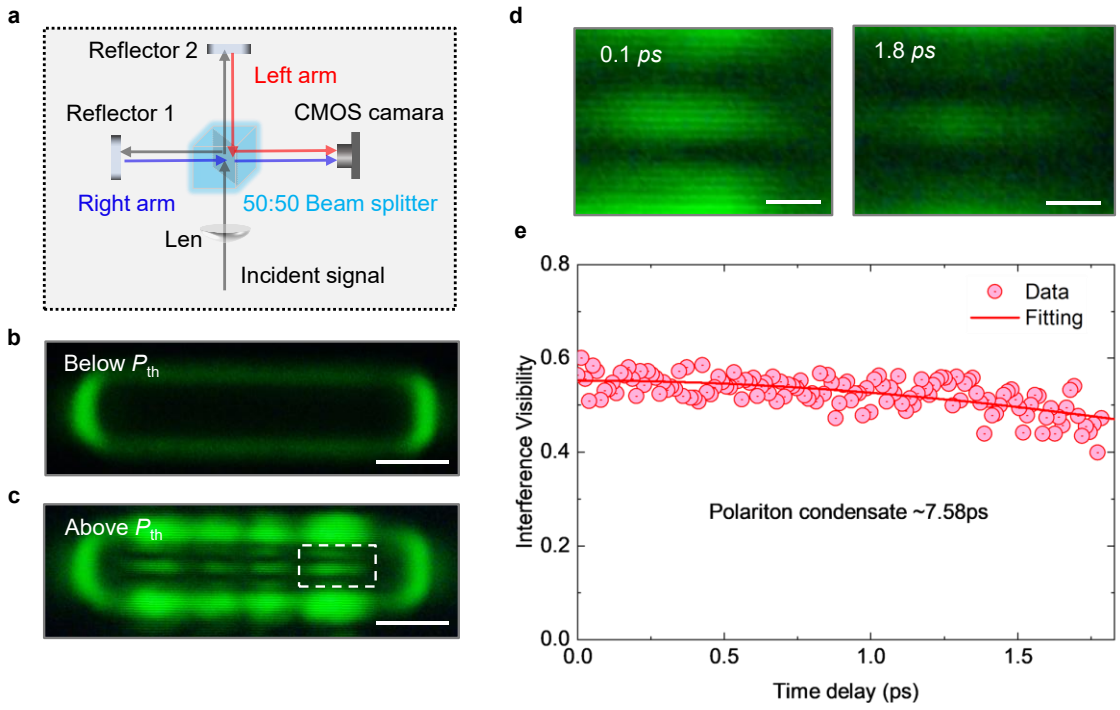

Figure S7 Coherence of EP condensates revealed by Michelson interference patterns under

1 kHz pulsed-laser excitation at room temperature (a) Schematic illustration of the Michelson interferometer. **(b)** Interference image of spontaneous photoluminescence from the $CsPbBr_3$ microwire below threshold at zero time delay. Scale bar: 2 μm. **(c)** Interference image of the EP condensate above threshold at zero time delay. Scale bar: 2 μm. **(d)** Local interference fringes at time delays of 0.1 ps and 1.8 ps, taken from the region marked by the white dashed box in (c). Scale bar: 300 nm. **(e)** Temporal evolution of the interference visibility, yielding a coherence time of 7.58 ps.

8. Dual-beam excitation configuration

To establish well-defined initial EP states for the subsequent logic operations, we implemented a dual-beam excitation configuration based on a 400 nm pulsed laser at a repetition rate of 1 kHz. The excitation beam was divided into two paths using a beam splitter and a delay line. One path was shaped into a ring-shaped signal beam by combining an axicon (AX2505, Thorlabs) with a Galilean telescope (BE02-UVB, Thorlabs), while the other path was focused into a spot-shaped gate beam using an f = 150 mm len together with a spatial aperture for beam selection. The temporal delay between the two beams was controlled by a delay line with a maximum travel range of 15 mm. The excitation beams and white-light illumination were focused onto the sample through a ×50 objective (Olympus, NA = 0.8). The reflected and emitted signals were collected by a 4f Fourier-imaging system, spatially filtered with an adjustable aperture, and directed into a spectrometer for *k*-space imaging, while a beam splitter simultaneously enables real-space imaging.

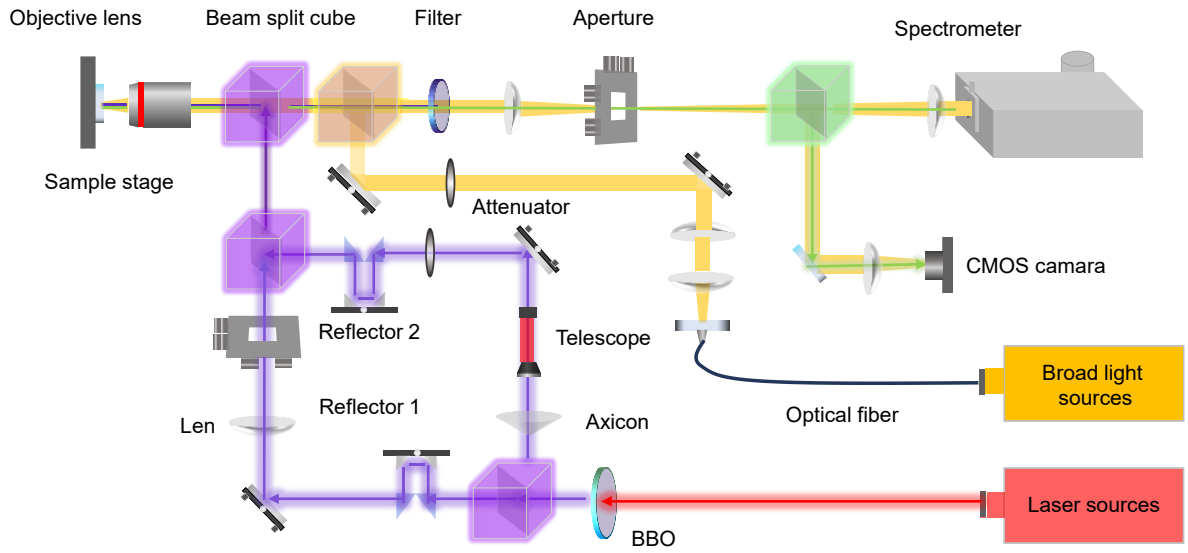

Figure S8 Schematic of the optical setup for angle-resolved photoluminescence spectroscopy incorporating the dual-beam excitation scheme. The red line represents the 800 nm laser emitted from the femtosecond source. The purple lines indicate the 400 nm beam generated after the 800 nm pulse passes through a BBO crystal, which is subsequently divided by a beam splitter and shaped into a ring-shaped signal beam and a dot-shaped gate beam. The yellow lines denote the white-light absorption and illumination path, while the green lines represent the photoluminescence and condensate emission from the $CsPbBr_3$ microcavity, which are finally collected by the spectrometer.

9. Ring-diameter-dependent discrete EP states

Next, we examined how the ring-shaped signal beam defines the initial distribution of EP condensates inside the optical trap. The ring-shaped excitation creates an excitonic potential barrier, while the EP flow propagates along the inner boundary of the trap and forms discrete states in the central region. Condensation preferentially occurs on the discrete states that best match the standing-wave modes formed by the confined propagation of EPs.

Angle-resolved photoluminescence spectra collected at different ring diameters D, ranging from 10 μm to 3 μm, show that as D decreases, the propagation distance of the EP flow is reduced and becomes matched to the standing-wave modes from $n = 5$ to $n = 1$. The corresponding photoluminescence spectra further reveal a clear shift of the dominant emission peak. Therefore, by varying the ring diameter D, the initial EP state corresponding to the '10' input can be controllably defined.

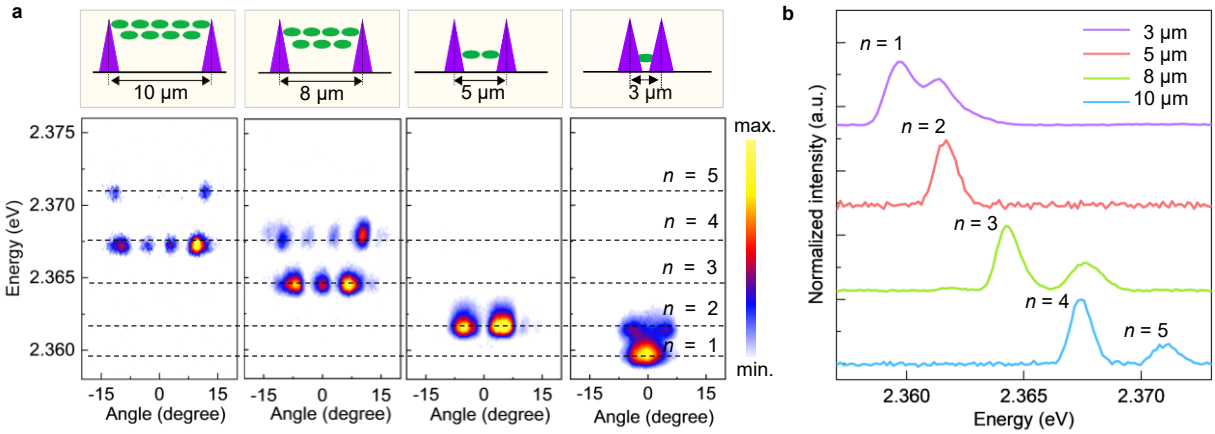

Figure S9 Ring-diameter-dependent angle-resolved photoluminescence spectra and condensation state distribution of EPs. (a) Angle-resolved photoluminescence spectra collected at ring diameters of 10, 8, 5 and 3 μm under 400 nm pulsed excitation (1 kHz) at room temperature. The schematics above the spectra illustrate the corresponding potential widths (indicated by purple triangles) and discrete EP states (green dots). **(b)** Corresponding photoluminescence spectra, with the positions of the discrete EP states marked by gray dashed lines.

10. Power-dependent discrete EP states

We then investigated the evolution of the discrete EP states with increasing signal-beam power. When the signal-beam power P_s is close to the threshold, the condensates predominantly occupy the $n = 5$ state, corresponding to the long-range propagation of EP flows along the x-axis. As P_s increases, enhanced EP scattering promotes relaxation toward $n = 1$ state. Meanwhile, the excitonic potential barrier induced by the signal beam gradually expands, reducing the central trap region and generating EP flows with progressively shorter propagation distances. As a result, the condensate distribution evolves from the $n = 5$ state to the $n = 4$, 3, 2, and 1 states. At 2.2 P_{th}, five discrete EP states are simultaneously occupied.

The synchronous blueshift with increasing excitation power is further confirmed from the extracted energy distributions. Together, the excitation geometry and pump intensity of the ring-shaped signal beam provide precise control over the initial EP distribution, thereby defining well-resolved starting conditions for multiple logic operations.

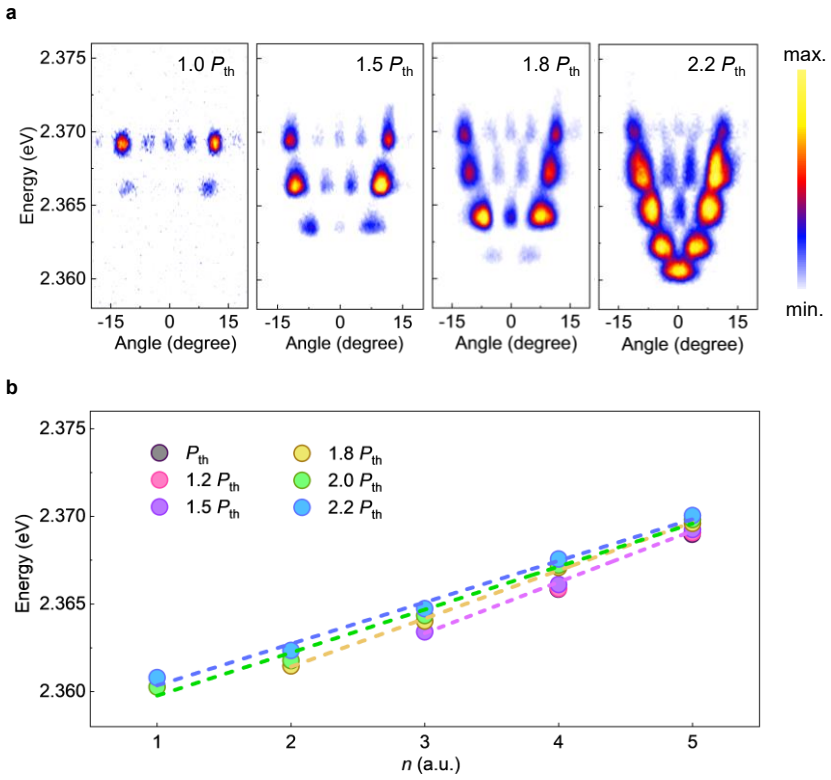

Figure S10 Power-dependent angle-resolved photoluminescence spectra and condensation state distribution of EPs. (a) Angle-resolved photoluminescence spectra obtained at different excitation powers of 1.0 P_{th}, 1.5 P_{th}, 1.8 P_{th}, and 2.2 P_{th}, showing the evolution of the discrete EP states with increasing pump intensity. Excitation source: 400 nm, 1 kHz pulse laser at room

temperature. **(b)** Energy distribution of discrete EP states at different excitation powers.

11. Distal output delivery and cascadability of EP logic operations

We further examine whether the logic output can be effectively delivered to the end of the microwire. This capability is essential for cascading multiple logic units in integrated polaritonic circuits. To verify this, photoluminescence spectra were collected from both the excitation region and the end region of the microwire under 400 nm pulsed excitation at a repetition rate of 1 kHz at room temperature. The Gaussian-fitted emission peaks collected at the end of the microwire remain well aligned with those collected inside the trap, indicating that the spectral signature of the condensates is preserved during propagation. This result demonstrates that the logic output can be delivered to the end of the microwire without spectral distortion, providing a key prerequisite for cascaded EP logic operations.

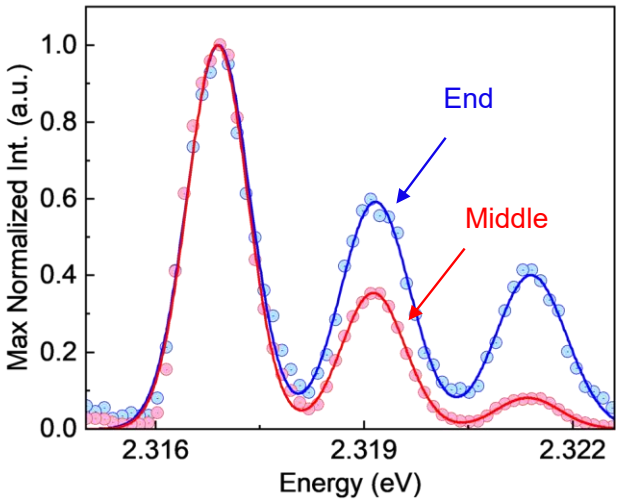

Figure S11 Cascadability of EP logic gates. Normalized photoluminescence spectra collected from the signal-beam region and the guided output outside, verifying the cascaded capability of the logic gate. Excitation source: 400 nm, 1 kHz pulse laser at room temperature.